Highly ordered, self-assembled monolayers of a spin-crossover complex with in-plane interactions

Zheng, S.; Spa, S.; Geest, E.P. van; Ruitenbeek, J.M. van; Bonnet, S.A.

EurJIC
European Journal of Inorganic Chemistry

Full Papers
doi.org/10.1002/ejic.202100290

Chemistry Europe
European Chemical Societies Publishing

Highly Ordered, Self-Assembled Monolayers of a Spin-Crossover Complex with In-Plane Interactions

Sipeng Zheng,[a] Silvia Spa,[a] Erik P. van Geest,[a, b] Jan M. van Ruitenbeek,[b] and Sylvestre Bonnet*[a]

For the technological integration of molecular switches in electronic devices, self-assembling nanomaterials of such switches are highly sought after. The syntheses of a new tetrapyridyl ligand bearing a C12 alkyl chain and two N–H bridges (compound **1**) and of its iron(II) complex [Fe(**1**)$(NCS)_2$] (compound **2**), are described. Magnetic susceptibility data for bulk samples of **2** confirmed their gradual spin-crossover properties. The self-assembly of **1** and **2** on highly ordered pyrolytic graphite surfaces (HOPG) was investigated by Scanning Tunneling Microscopy (STM). Both compounds **1** and **2** formed ordered monolayers after deposition by drop casting. The patterns of the two compounds are very different, which is attributed to the fundamentally different hydrogen bonding networks before and after coordination of $Fe(NCS)_2$ to the tetradentate chelate. Two possible models for the self-assembly of **1** and **2** are provided. This work suggests that it is possible to design molecular switches that self-assemble on surfaces in highly ordered monolayer films. This is a significant step in the development of spin-switching materials, which may streamline the integration of molecular switches in for example memory and sensing devices.

Introduction

The design of molecular switches that can be utilized for information processing and data storage is an attractive goal in material science. Spin-crossover (SCO) compounds hold interesting potential in this field. SCO can occur for $3d^4$–$3d^7$ transition metal ions in a pseudo-octahedral environment, *i.e.*, when the *d*-electrons can occupy either a high-spin (HS) or a low-spin (LS) state configuration. SCO can be triggered by temperature variations, light irradiation, or by the application of pressure, of a magnetic field, of an electric field.[1] The ability to switch these material with high control makes them highly promising technological materials, *i.e.* as molecular switches, display materials and sensing entities.[2–4] Indeed, extensive research efforts have already yielded various devices based on SCO materials, notably actuators and microelectromechanical devices (MEMS),[5–7] sensors,[8–10] and memory devices.[11–14] At the same time electrical SCO-readout platforms (based on for example the 2D semiconductor material graphene) were developed for the integration of the typically insulating SCO materials in electronic systems.[15–18]

Current spin-crossover research is driven by the pursuit of such electronic devices at the nanoscale; hence a plethora of nanoparticles, thin films, liquid crystals and surface patterns of spin-crossover materials have been described.[19] Of particular interest are highly-ordered, self-assembled nanostructures.[2,20–22] For example, metal complexes with long alkyl chains were shown to self-assemble into structured multifunctional nanomaterials,[23–28] *i.e.*, materials in which several properties are combined, such as SCO and liquid crystal behavior[23,29–31] or magnetic exchange interactions,[32] as well as single-molecule magnet (SMM) properties.[33] In all cases, examples have shown that the self-assembly of such molecules to surfaces using the bottom-up approach was a new and powerful tool to prepare devices,[34–35] which might be complementary to more traditional top-down microfabrication techniques.[34] However, the bottom-up self-assembly of one- or two-dimensional arrays of molecules with controlled magnetic properties requires the detailed understanding and control of *inter*-molecular forces.

Previously, we reported the mononuclear SCO compound [Fe(bapbpy)$(NCS)_2$] (bapbpy = *N,N'*-di(pyrid-2-yl)-2,2'-bipyridine-6,6'-diamine) to be highly cooperative,[36] and more recently electrically probed the spin switches in single crystals of this compound.[15] Intermolecular interactions are well characterized for this compound in the bulk, where hydrogen bonding interactions play a critical role for the high cooperativity between the SCO molecules in the crystalline material, which is a consequence of intermolecular interactions in the crystal lattice.[37] High cooperativity is important for fast, hysteretic transitions, which is usually considered as important for information storage applications.[38] Intermolecular N–H···S hydrogen bonds between neighboring molecules are indeed correlated with the occurrence of hysteretic SCO. Based on these studies, a new N_4-donor ligand **1** was designed (Figure 1). This tetradentate ligand consists of a bapphen (*N,N'*-bis(pyrid-2-

[a] Dr. S. Zheng, S. Spa, Dr. E. P. van Geest, Prof. Dr. S. Bonnet
Leiden Institute of Chemistry, Leiden University,
Gorlaeus Laboratories, P.O. Box 9502, 2300 RA Leiden, The Netherlands
E-mail: bonnet@chem.leidenuniv.nl
[b] Dr. E. P. van Geest, Prof. Dr. J. M. van Ruitenbeek
Leiden Institute of Physics, Leiden University,
Kamerlingh Onnes Laboratory, Niels Bohrweg 2, 2333 CA Leiden, The Netherlands

Supporting information for this article is available on the WWW under https://doi.org/10.1002/ejic.202100290

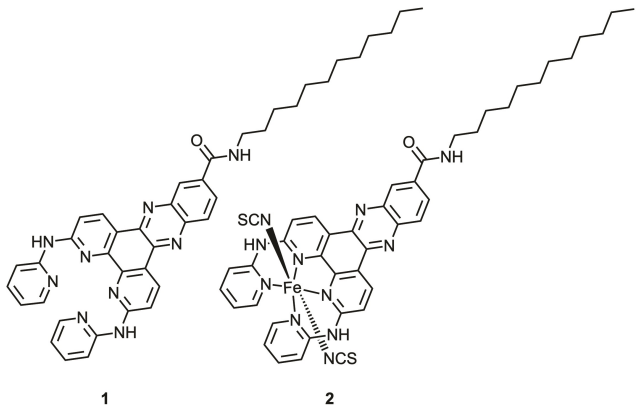

Figure 1. Chemical structures of ligand **1** and its iron(II) complex **2**.

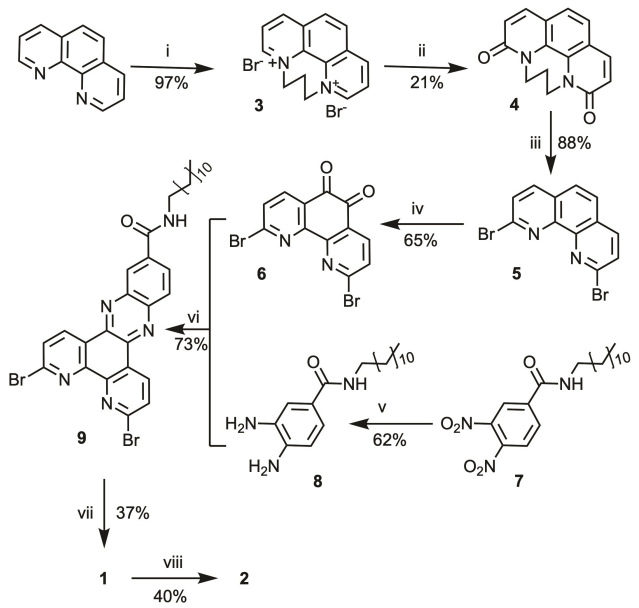

Figure 2. Synthetic route towards compounds **1** and **2**. (i) 1,3-dibromopropane, $PhNO_2$, 120 °C, 4 h. (ii) $K_3[Fe(CN)_6]$, NaOH, H_2O, RT, 4 h. (iii) $POBr_3$, PBr_3, 192 °C, 18 h. (iv) KBr, conc. H_2SO_4, conc. HNO_3, 80 °C, 4 h. (v) Pd/C 10%, H_2, MeOH, RT, 5 h. (vi) MeOH, 85 °C, 18 h. (vii) 2-Aminopyridine, 2.7 mol% $Pd(dba)_2$, 2.7 mol% (S)-BINAP, 2 eq.Cs_2CO_3, dry toluene, 110 °C, 4 d. (viii) 1.1 eq. 0.1 M $Fe(NCS)_2$, MeOH, 80 °C, 18 h, under argon atmosphere.

yl)-1,10-phenanthroline-2,9-diamine) ligand to which a long alkyl chain (C_{12}) is attached *via* aromatic rings in positions 5 and 6 of the phenanthroline ring. The synthesis of **1** and its complexation to iron(II) bisthiocyanate is described, as well as the SCO properties of [Fe(**1**)$(NCS)_2$] (complex **2**) in the bulk. The compounds were then deposited on highly oriented pyrolytic graphite (HOPG) surface by drop casting, and the self-assembly of ligand **1** and of its iron complex **2** on HOPG was studied by scanning tunneling microscopy (STM) techniques, revealing the formation of highly ordered monolayers.

Results and Discussion

Synthesis

An overview of the synthesis of ligand **1** is given in Figure 2. First, 2,9-dibromophenanthroline (**5**) was synthesized according to literature procedures.[39–40] The positions α to the nitrogen atoms were activated towards nucleophilic attack by quaternizing the nitrogen atoms with a propane bridge (compound **3**). Subsequent oxidation with $K_3[Fe(CN)_6]$ afforded compound **4** in 21% yield. Bromination of the 2 and 9 positions was realized with a $PBr_3/POBr_3$ mixture yielding compound **5** in 88% yield. The 5,6-dione functional groups were then introduced according to a method described by Ishi-i *et al*[40] using a mixture of H_2SO_4, HNO_3 and KBr. Compound **6** was obtained in a reasonable yield of 65% (Figure 2).

The next step of the synthesis involved the attachment of an alkyl chain to the 5,6-dione groups of **6**. The diamine compound **8** which contained a 12-carbon alkyl chain, was synthesized by modifying a two-step procedure described by Ikeda et al (Figure 2).[41] The formation of pyrazine ring of **9** was then achieved by refluxing **6** and **8** in methanol for 18 h.[42] **9** was then collected by filtration and obtained with a yield of 73%. Finally, the Buchwald-Hartwig cross-coupling reaction between compound **9** and 2-aminopyridine afforded compound **1** in 37% yield (Figure 2).

The coordination of compound **1** to iron(II) thiocyanate to form complex **2** was achieved by adding a slight excess of a methanolic solution of $Fe(NCS)_2$ to a methanol suspension of **1** (Figure 2). Initial attempts of complexation were performed at room temperature for 18 h under argon. In these conditions a yellow solid was obtained that later proved to be lower in purity and contained some uncoordinated NCS^- ligands as shown by their stretching vibrations at 2051 cm^{-1} in the IR spectrum of the product (see Figure S1, ESI).[43] It appeared that heating to 80 °C was necessary for the coordination reaction to go to completion. After refluxing the mixture at 80 °C for 18 h under argon, a brown solid was obtained 40% yield. The new iron(II) complex **2** was analyzed with mass spectrometry, elemental analysis, and IR spectroscopy. Elemental analysis could not be strictly fitted with the formula of the compound, which highlights the difficult purification of these compounds, as they cannot be purified by chromatography of HPLC and only rely for purification on recrystallization. However, fitting with methanol lattice molecules came close to the expected elemental composition (C 57.08, H 6.29, N 15.25 found, C 57.96, H 6.08, N 13.73 calc). In addition, electron-spray mass spectroscopy clearly showed the expected $[Fe(\mathbf{1})]^{2+}$ dicationic peak (calculated at *m/z* 366.6465 for $[Fe(\mathbf{1})]^{2+}$), which confirmed coordination of the ligand to the Fe(II) ion. Consistently, the IR spectrum showed the characteristic stretching vibrations of the coordinated thiocyanate ligands at 2077 cm^{-1} for **2**. Overall, combined analysis pointed to a purity of around >90% for **2**, and all further experiments were performed with this material.

Magnetic susceptibility measurement of 2 in the bulk

In order to investigate the magnetic properties of compound **2** the temperature dependence of $\chi_M T$ was measured in both the heating and the cooling modes (Figure 3, where χ_M = the molar magnetic susceptibility and T = temperature). Compound **2** showed a gradual and incomplete SCO behavior in the measured temperature range (5 to 350 K), with no hysteresis cycle. The $\chi_M T$ value of 2.5 $cm^3 K mol^{-1}$ at 300 K gradually decreases to 1.5 $cm^3 K mol^{-1}$ at 100 K, where it reaches a plateau. Further decreasing of $\chi_M T$ below 50 K is due to the zero-field splitting. The transition temperature of **2**, measured as the maximum of $d\chi_M T/dT$ vs. T (see Figure S2, ESI), was 182(25) K in both the heating and the cooling modes. The $\chi_M T$ value of 2.5 $cm^3 K mol^{-1}$ at 300 K was low compared to the expected value of 3.0 $cm^3 K mol^{-1}$ for an HS iron(II) center in an octahedral FeN_6 environment, which was consistent with the presence of bulk impurities observed by elemental analysis.

STM spectroscopy of compounds 1 and 2 on HOPG surfaces

Highly oriented pyrolytic graphite (HOPG) was chosen as a surface for the study of the self-assembly of **1** and **2**. The deposition of **1** or **2** on a HOPG surface was realized by adding a drop of a DMF solution of compound **1** or **2** (80 nM) and evaporating the solvent under a flow of argon. The self-assembly of compound **1** or **2** on HOPG was then studied using STM. For both compounds highly ordered structures were observed (Figure 4), characterized by alternating bright and slightly darker stripes, whereas these stripes were absent from a control sample that was prepared in absence of both compounds. For **1** on HOPG, the periodicity of the stripes was estimated at 4.0 nm with the bright stripes exhibiting a width of 1.6 nm, and the darker stripes a width of 2.3 nm (Figure 4). In STM images a brighter color represents a larger apparent height of the structure. The apparent height is a combination of the actual height and increased current due to a higher local density of states. For compounds having aromatic groups the latter effect often dominates and bright spots are associated with the aromatic units. Thus, we tentatively assign the bright stripes to the aromatic unit of **1** (the bapphen part) because of the presence of π-electrons in aromatic rings.[44–45] The darker stripes are assigned to the alkyl chains in **1**, which have low-lying sigma orbitals that poorly contribute to the observed current. These observations are consistent with other reports showing similar patterns for aromatic compounds with long alkyl tails[34,46–47]

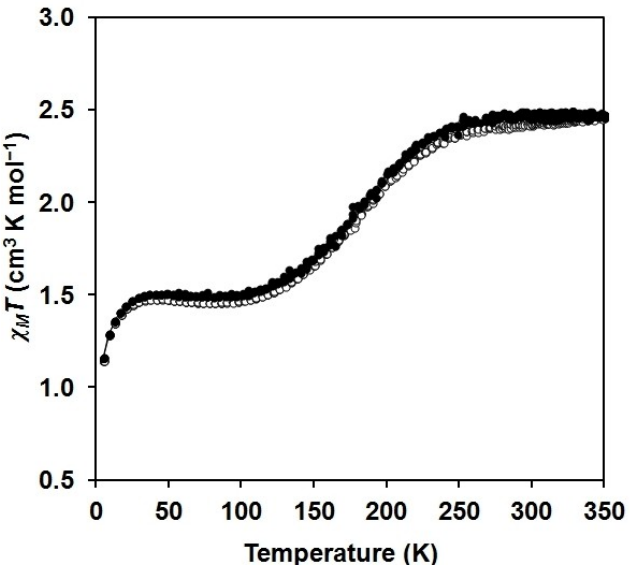

Figure 3. Plot of $\chi_M T$ versus T for compound **2** in both heating (empty circle) and cooling mode (filled circle). The measurement was performed with steps of 5 K in the low temperature range and with steps of 2 K in the 250 and 350 K temperature range, with a scan rate of 0.3–1.1 K min^{-1}.

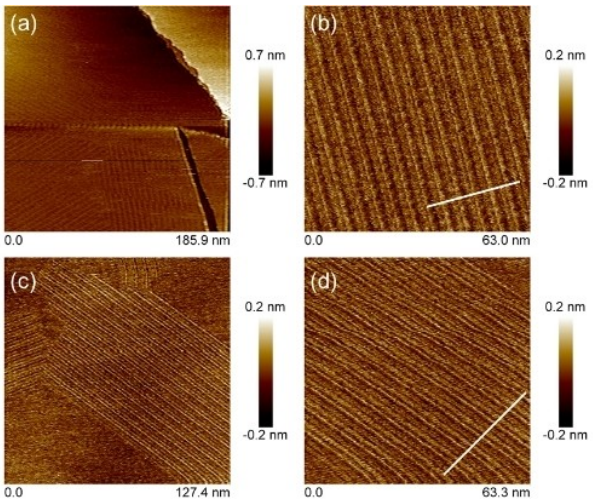

Figure 4. STM images of thin layers adsorbed on HOPG surface for: (a) compound **1**, 185.9 nm × 185.9 nm; (b) compound **1**, 63 nm × 63 nm, a separate STM image taken after a zoom-in of (a); (c) compound **2**, 127.4 nm × 127.4 nm; (d) compound **2**, 63.3 nm × 63.3 nm, a separate STM image taken after a zoom-in of (c) The brightness is proportional to the height at constant current mode. Both **1** and **2** on HOPG show ordered 2D domains, the white lines indicated in (b) and (d) are for stripe-width analysis in Figure 5. All images were taken under the same conditions: V_{bias} = + 500 mV, I_{set} = 1 nA.

Compound **2** also self-assembles on HOPG forming small islands of highly ordered structures (Figure S4, ESI). Images of smaller size (Figure 4d) showed alternating bright and slightly darker stripes just like for **1**. However, the periodicity of **2** seems smaller than that of **1** (Figure 4b vs. 4d), which was confirmed by analyzing the width of the stripes (Figure 5). Although the signal-to-noise ratio appears to be higher than for **1**, the periodicity of the stripes was estimated to be 2.0 nm, with one bright stripe of 1.0 nm and one dark stripe of 1.0 nm. Like for **1**, the bright stripes are assigned to the aromatic unit of **2** (the bapphen part), and the darker stripes are assigned to the alkyl chains in **2**. The shortening of the width of both bright and dark stripes in **2** on HOPG remains intriguing, and this suggest that the surface self-assembly of compound **1** is influenced by coordination of the ligand to iron. This effect could possibly occur as an effect of intermolecular interactions between the

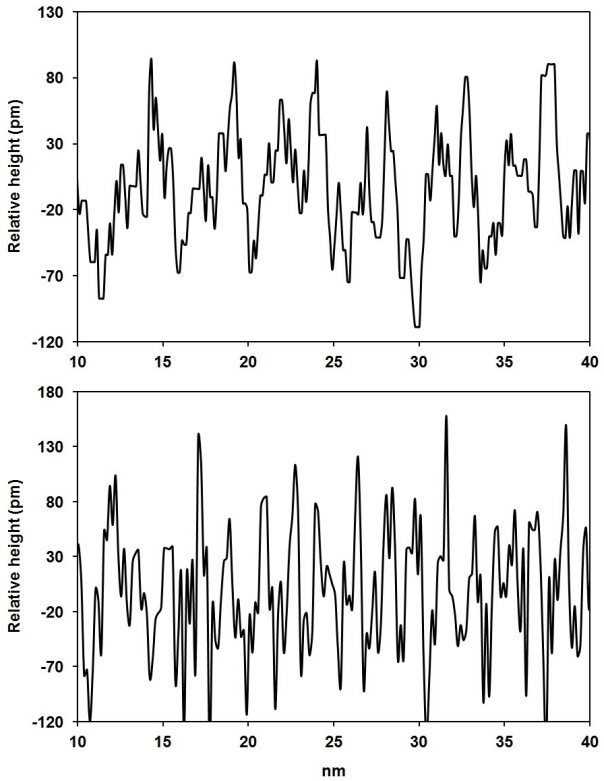

Figure 5. Stripe-width analyses for ligand **1** (top, from Figure 4b) and complex **2** (bottom, from Figure 4d) on HOPG along the white lines in Figures 4b and 4d. Sections of 30 nm are shown instead of the entire length of the lines to ease comparison.

NCS and bapphen ligands, or of two NCS ligands of neighboring complexes in the crystal packing of the monolayer.

Discussion

The $\chi_M T$ vs. T plot for compound **2** in the bulk shows gradual and incomplete spin transition behavior, with a relatively high residual HS fraction at low temperature. As examples previously reported,[48–49] high residual HS fractions are expected for non-cooperative SCO with low $T_{1/2}$. The gradual spin transition suggests rather weak intermolecular interactions between the iron complexes.[50] On the one hand, compound **2** possesses two N–H bridges susceptible to engage in N–H···S hydrogen bonding networks, and we expected to observed more cooperativity in the bulk. On the other hand, the very incomplete nature of the thermal SCO may be attributed on the one hand to its gradual character, coupled to the low SCO temperature. While it is not uncommon for precipitated SCO materials to have less cooperative SCO than their crystallized version, for other SCO systems a loss of cooperativity and/or more incomplete transition can be observed upon ageing, solvent loss, or amorphization. Here the bulk 3D material **2** could not be crystallized and was isolated as a precipitated powder; we hypothesize that its gradual and incomplete SCO may at least in part be associated to a lack of crystallinity.

From the IR spectra of cooperative SCO compounds such as [Fe(bapbpy)$(NCS)_2$], which shows short N···S distances and strong N–H···S hydrogen bonds, multiple absorption bands for the stretching vibrations of the N–H bond are observed between 3000 and 3300 cm^{-1}. In contrast, for gradual SCO compounds such as [Fe(Me_2bapbpy)$(NCS)_2$] the N···S distances are longer and the N–H···S hydrogen bonds are weaker,[51] which translates in the IR spectrum of the solid into a single, stronger absorption band around 3400 cm^{-1}. Therefore, the multiple absorption bands in **2** may indicate that N–H···S interactions be present in the bulk. The lower cooperativity of the SCO in **2** might be a consequence of other inter-molecular interactions, such as π-π stacking between the large aromatic rings and/or Van der Waals interactions between the hydrophobic tails. Overall, the iron-to-iron intermolecular distances might be longer in **2** than in [Fe(bapbpy)$(NCS)_2$], which would explain the lack of cooperativity for this compound. This effect is similar to the metal dilution effect shown in [Fe_xZn_{1-x}-(bapbpy)$(NCS)_2$],[52] where increasing concentrations of the magnetic inert Zn ions in the crystal lattice causes the iron centers to become further away from each other, resulting in a lowered cooperativity for SCO.

Following deposition on HOPG it is immediately clear from STM images that the molecules of **1** and **2** form complex and highly ordered structures with long-range order. Comparing with the STM image obtained from a freshly cleaved HOPG surface (Figure S3) these ordered structures are not associated to, and do not follow, the underlying step edges of the HOPG surface. These features are somewhat reminiscent of the ordered structures reported recently for other alkyl-functionalized compounds.[34]

In a possible model for the arrangement of **1** on HOPG, the bright stripes are formed by the aromatic part of **1**, which may lay flat on the surface and interact *via* hydrogen bonding between neighboring molecules. Indeed, the terminal pyridine rings in **1** can rotate in such a way that its nitrogen atom acts as an H-bond acceptor, while the N–H bridge of the neighboring molecule acts as a H-bond donor (Figure 6). In our model, the alkyl chains also lie flat on the surface and form interdigitated domains that correspond to the dark stripes observed by STM. To evaluate the relevance of this model, the molecular structure of **1** was calculated by DFT in vacuum using the B3LYP functional and the LANL2DZ basis set as implemented in the GAMESS-UK package (Figure 7).[53] From the 3D structure of ligand **1** the calculated width of the aromatic part of the 2D network on HOPG should be about 1.6 nm, a distance measured from projections of the nitrogen atom on the central pyrazine ring to the nitrogen atom on the pyrazine ring of a neighboring molecule (Figure 6). This value fits well with the experimental width analysis of the bright stripe (*ca.* 1.6 nm, Figure 5). The length of the alkyl chain in **1**, in which the distance measured from the tip of the tail to the nitrogen atom on the central pyrazine ring, is also close to the observed width of the dark stripes (2.3 nm, Figure 6). Overall, ligand-to-ligand hydrogen bonding and strong interactions with the surface may create an interdigitated 2D-assembly of flat ligands **1** on

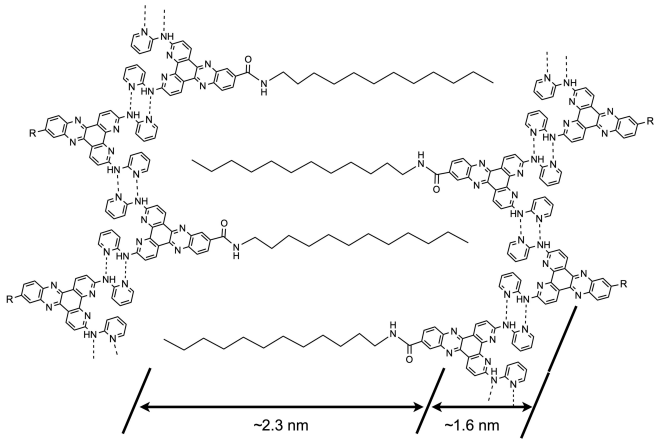

Figure 6. Proposed model for the self-assembly of **1** on HOPG (R = CONH $(CH_2)_{11}CH_3$). Distances are calculated using Mercury,[56] and the molecular structure of **1** is based on DFT. The 1D supramolecular chains are stabilized by H-bonding between the N–H bridge and the N atom on the terminal pyridine of the neighboring molecule (insert); These chains form a 2D motif stabilized by van der Waals interactions between the alkyl tails.

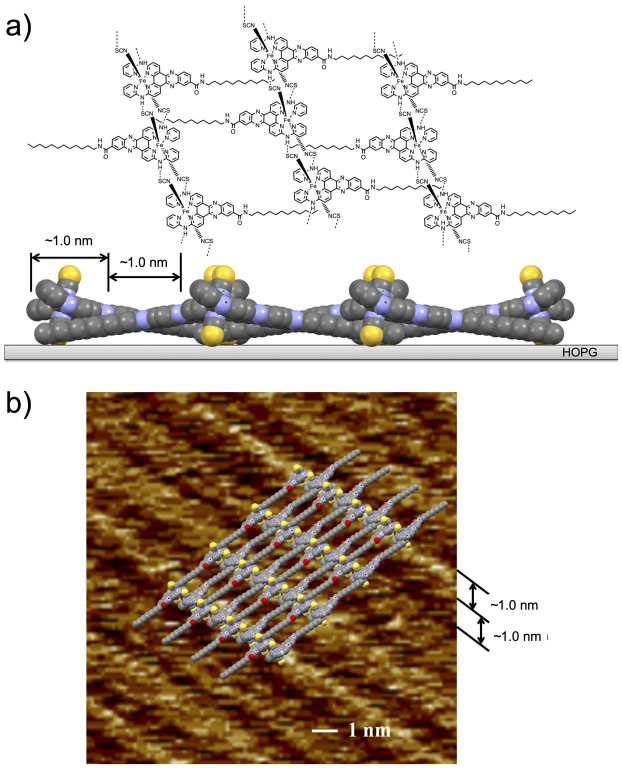

Figure 7. (a) Proposed model for the arrangement of **2** on HOPG: (top) schematic representation of intermolecular N–H···S interactions between neighboring iron(II) complexes; (bottom) side view of the arrangement of **2** parallel to the graphite surface. The two thiocyanate ions are modelled roughly perpendicular to the basal graphite plane. The distances are calculated using the program Mercury[56] and the molecular structure of **2** calculated by DFT (color code: gray, carbon; red, oxygen; yellow, sulfur; blue, nitrogen). (b) A zoom-in STM image from Figure 7.2d, with an overlay of the proposed model highlighting the positions of the 1D supramolecular chains (color code: gray, carbon; red, oxygen; yellow, sulfur; blue, nitrogen).

HOPG, which is also consistent with previously reported adsorption of pyridines on the carbon layer of HOPG.[54–55]

Clearly a shorter periodicity was found for the self-assembly of **2** on HOPG. To understand this observation, a model of the arrangements of **2** on the HOPG surface was built based on the molecular structure of **2** in the LS state obtained by DFT (Figure S5b). The structure of **2** was built from the X-ray structure of $[Fe(bapbpy)(NCS)_2]$ complex in the LS state.[36,51] The tetradentate ligand **1** coordinates to iron(II) in the equatorial plane, leaving the two thiocyanate ligands in the axial positions of the octahedron (Figure S5b). Thus, on HOPG the tetradentate ligand cannot lie flat because of the axial thiocyanate ligands that create a vacant space underneath **2**. As observed in many reported crystal structures of bapbpy-related iron(II) complexes, each complex may interact with two neighboring complexes inter-molecular N–H···S hydrogen bonds to form one-dimensional chains (Figure 7a) of arbitrary length. In addition, because of these N–H···S intermolecular interactions the molecules are forced to tilt with respect to the surface in order to optimize the contact between the monolayer and the basal plane of graphite. As a result, the alkyl chains might enter the vacant space created by the axial thiocyanate ligands and the tilt, to ensure a close contact between the surface and the molecular network (Figure 7a). In such a model, the periodicity of the 2D network would be shorter than the length of one molecule of **2**. From geometrical estimations the calculated widths of both the aromatic part and of the alkyl chains would fit well with the shorter observed width of the stripes of the network (Figure 7a–b). Overall, IR spectroscopy of the bulk as well as the STM images of **2** on HOPG suggest that N–H···S hydrogen interactions do occur in the monolayers of **2**, giving rise to highly ordered 2D supramolecular structures. Importantly, these results suggest that SCO in these films could be cooperative; however, we could not measure this at this point. We interpret the fact that bonding of **2** on HOPG forms 2D domains as a demonstration that N–H···S hydrogen interactions might govern intermolecular contacts in a monolayer domain, whereas recent examples of other iron-based compounds showing intercalation of C_{12} ligand chains and π-π interactions but lack of N–H···S hydrogen interactions were shown to form isolated 1D nanostructures on surface.[57–58]

Conclusions

The new bapphen-based ligand **1**, bearing a 12-carbon chain at the back of the phenanthroline backbone, was designed to self-assemble a SCO iron complex on surfaces. Its iron(II) complex **2** shows in the bulk a gradual spin transition with no hysteresis cycle. STM images of both ligand **1** and complex **2** on HOPG revealed stable and highly ordered arrangements on the surface. The different periodicities observed in STM images are attributed to the two different types of intermolecular interactions in **1** and **2**: N–H···N hydrogen bonding for **1** vs. N–H···S hydrogen bonding for **2**. Although the STM images at room temperature and ambient pressure show a clear ordering of **2** on HOPG, the resolution of the images does not give enough

information to exactly determine the structure of the monolayer, which remains a challenge for the future. Importantly, the existence of the in-plane N–H···S interactions in the monolayer films of **2** suggests that SCO of the molecules in the film may show some form of cooperativity, in spite of lack of signs of hysteresis in the magnetic susceptibility data of the bulk material. Overall, the present results show that the introduction of long alkyl chains into the ligand bapphen without blocking the N–H bridges is a valid strategy to deposit and organize SCO molecules onto surfaces. Albeit information about the exact spin crossover properties of these molecules in a monolayer ordering remain unknown for now, highly ordered self-assembled molecular switches like compound **2** may provide a good basis for building molecular data storage devices where each molecule bear a bit (or q-bit) of information.

Experimental Section

All reactions were performed under argon atmosphere using standard Schlenk line techniques. The applied vacuum was about 10^{-3} mbar. Dry solvents were collected from a Pure Solvent's MD5 dry solvent dispenser from Demaco. Degassed solvents were obtained by bubbling argon through 50 mL solvent in a Schlenk flask for one hour. For all complex syntheses, degassed solvents were used. The compounds **3**, **4**, 2,9-dibromo-1,10-phenanthroline (**5**) and 2,9-dibromo-1,10-phenanthroline-5,6-dione (**6**) were synthesized using literature procedures[39–40,59] All other chemicals were obtained from commercial sources and used without any further purification. Thin-layer chromatography was carried out on silica TLC Al foils N/UV_{254} from Sigma Aldrich or on pre-coated TLC-sheets Alugram® Alox N/UV_{254}. Flash chromatography was performed using silica gel (Sigma Aldrich, silica gel 60 Å 230–400 mesh) or aluminium oxide (Sigma Aldrich, activated, neutral, Brockmann I, 58 Å). Filtrations of ligands and complexes were carried out using Whatman RC60 membrane filters. NMR Spectra were measured on a Bruker DPX-300 Spectrometer at room temperature unless otherwise specified. Chemical shifts are indicated in *ppm* relative to TMS. Mass spectra were obtained using soft electron-spray from a Thermoquest Finnagen TSQ-quantum instrument. HR Mass spectra were measured using direct injection (2 μL of a 2 μM solution in DMF and 0.1% formic acid on a mass spectrometer (Thermo Finnigan LTQ Orbitrap) equipped with an electron-spray ion source in positive mode (source voltage 3.5 kV, sheath gas flow 10, capillary temperature 275 °C) with resolution R = 60.000 at m/z = 400 (mass range = 150–2000) and dioctyl phthalate (m/z = 391.28428) as "lock mass". IR spectra were acquired with a Perkin-Elmer Spectrum Two FT-IR spectrometer. Elemental analyses (C,H,N,S) for compounds **7** and **8** were obtained from a Perkin-Elmer 2400 Series II analyzer (Leiden University), and for compounds **1**, **2** and **9** were performed by Kolbe Mikroanalytisches Laboratorium, Mülheim an der Ruhr, Germany.

Compound 7: To an ice-cold suspension of 3,4-dinitrobenzoic acid (1.0 g, 4.7 mmol) and oxalylchloride (0.45 mL, 5.2 mmol) in dry DCM (40 mL), DMF (0.1 mL, 20 mol%) was added drop wise, which gas evolution was observed. After stirring for 1 h at room temperature the solvent was evaporated to remove the excess of oxalylchloride. The remaining solid was redissolved in dry DCM (25 mL) and added slowly at 0 °C to a solution of dodecylamine (961 mg, 5.18 mmol) and triethylamine (0.98 mL, 7.1 mmol) in dry DCM (25 mL). The reaction mixture was stirred overnight at room temperature, and a clear yellow solution was obtained. Then the yellow solution was washed with brine (2 × 25 mL), the organic layer was dried over $MgSO_4$, after filtration to remove $MgSO_4$, and subsequently evaporated the solvent under reduced pressure, an orange solid was obtained. The solid was subjected to column chromatography (silica gel, 0.5% MeOH/DCM, 200 mL) eluting with 2% MeOH/DCM. The third fraction was collected (R_f = 0.2, 2% MeOH/DCM) and compound **7** was obtained as a yellow solid (41%, 731 mg). ESI-MS m/z (calc): 380.21 (380.4 $[M+H]^+$). ^{1}H NMR (300 MHz, MeOD) δ 8.48 (d, *J* = 1.8 Hz, 1H; H-5), 8.28 (dd, *J* = 8.4, 1.8 Hz, 1H; H-3), 8.15 (d, *J* = 8.4 Hz, 1H; H-2), 3.40 (m, 2H; γ), 1.62 (d, *J* = 7.1 Hz, 2H; δ), 1.32 (d, *J* = 24.1 Hz, 18H; H-ε), 0.88 (m, 3H; H-ζ). ^{13}C NMR (75 MHz, MeOD) δ 165.56 (Cq), 140.95 (Cq), 133.70 (C-2), 126.84 (C-5), 125.40 (C-3), 106.00 (Cq), 41.46 (C-γ), 33.07 (C-ε), 30.76 (C-ε), 30.71 (C-ε), 30.67 (C-ε), 30.47(C-ε), 30.42 (C-ε), 30.24 (C-δ), 28.07 (C-ε), 14.44 (C-ζ). Not all quaternary carbons could be detected. Elemental analysis calcd (%) for $C_{19}H_{29}N_3O_5$: C 60.14, H 7.70, N 11.10; found: C 60.40, H 6.60, N 10.90.

Compound 8: Under an argon atmosphere, compound **7** (0.20 g, 0.53 mmol) and Pd/C 10% (30 mg, 0.28 mmol) were suspended in degassed methanol (25 mL). The solution was put under an H_2 atmosphere using a balloon filled with H_2 and stirred at room temperature for 5 h. After filtration over Celite and evaporation of the solvent, 171 mg of crude product was obtained. The solid was subjected to column chromatography (silica gel, 10% MeOH/DCM, 100 mL). By using 10% MeOH/DCM as eluent for the column as well for the TLC, the last spot (R_f = 0.1) was collected which contained the pure product as a gray solid (62%, 105 mg). ESI-MS m/z (calc): 320.1 (320.5 $[M+H]^+$), 342.1 (342.5 $[M+Na]^+$), 374.2 (374.5 $[M+MeOH+Na]^+$). ^{1}H NMR (300 MHz, MeOD) δ 7.14 (d, *J* = 2.0 Hz, 1H; H-5), 7.08 (dd, *J* = 8.1, 2.1 Hz, 1H; H-3), 6.65 (d, *J* = 8.1 Hz, 1H; H-2), 1.57 (t, *J* = 7.0 Hz, 2H; H-γ), 1.30 (d, *J* = 16.6 Hz, 20H; H-δ, ε), 0.87 (m, 3H; H-ζ). ^{13}C NMR (75 MHz, MeOD) δ 170.83 (C-α), 140.60 (C-4), 134.82 (C-6), 125.38 (C-1), 120.30 (C-3), 116.41 (C-5), 115.66 (C-2), 40.90 (C-γ), 33.09 (C-ε), 30.79 (C- δ), 30.78 (C-ε), 30.74 (C-ε), 30.70 (C-ε), 30.52 (C-ε), 30.49 (C-ε), 28.13 (C-ε), 23.75 (C-ε), 14.45 (C- ζ). Elemental analysis calcd (%) for $C_{19}H_{33}N_3O$: C 71.43, H 10.41, N 13.15; found: C 71.62, H 9.20, N 13.09.

Compound 9: Under an argon atmosphere, compound **6** (245 mg, 0.67 mmol) was suspended in degassed methanol (15 mL), compound **8** (214 mg, 0.67 mmol) was first dissolved in degassed methanol (15 mL), and then added to the yellow suspension of **6** slowly, a color change from yellow to red was observed. The red solution was stirred at 85 °C for 18 h, a milky brown suspension was obtained. After filtration and washed with MeOH (4 × 4 mL), compound **9** was dried for 3 h *in vacuo* and obtained as a light brown solid (73%, 316 mg). Compound **9** was used as it is without further purification. ESI-MS m/z (calc): 652.2 (652.1 $[M+H]^+$). ^{1}H NMR (300 MHz, CD_2Cl_2) δ 9.35–9.22 (m, 2H; H-4), 8.39 (s, 1H; H-10), 8.27–8.19 (m, 2H; H-7, 8), 7.99–7.91 (m, 2H; H-3), 7.13 (s, 1H; NH), 3.62 (t, *J* = 7.3 Hz, 2H; H-β), 1.93–1.68 (m, 2H; H-γ),), 1.64–1.09 (m, 20H; H-δ),), 0.87 (dd, *J* = 7.8, 5.2 Hz, 3H; H-ε). ^{13}C NMR (75 MHz, CD_2Cl_2) δ 166.92 (C=O), 146.16, 146.04, 143.48, 141.89, 137.94, 136.49 (C-4), 136.36 (C-3), 130.16 (H-8), 130.05 (C-7), 130.01 (C-4), 128.06 (C-10), 127.22, 127.16, 41.13 (C-β), 32.34 (C-δ), 30.10 (C-δ), 30.05 (C-γ), 29.82 (C-δ), 29.77 (C-δ), 27.55 (C-δ), 23.10 (C-δ), 14.29 (C-ε). Not all quaternary carbons could be detected. Elemental analysis calcd (%) for $C_{31}H_{33}Br_2N_5O{\cdot}KBr$: C 48.33, H 4.32, N 9.09; found: C 48.52, H 4.98, N 8.87.

Compound 1: A mixture of compound **9** (238 mg, 0.37 mmol), $Pd(dba)_2$ (6.7 mg, 0.012 mmol), (S)-BINAP (9.1 mg, 0.015 mmol) and Cs_2CO_3 (336 mg, 1.03 mmol) was put under argon and partially dissolved in degassed toluene (30 mL) in a dry round-bottom flask. The mixture was stirred at room temperature for 20 min and 6-amino-2,2'-bipyridine (72 mg, 0.76 mmol) was added, followed by heating the reaction mixture to 110 °C. After 3 days, the deep red mixture was cooled down to room temperature. Deionized water

(20 mL) was added, and the mixture was stirred for 1 hour. The resultant orange suspension was filtered and washed with H_2O (3× 4 mL). After drying under high vacuum, 343 mg of crude product was obtained. The crude solid was subjected to column chromatography (silica gel, 5% MeOH/DCM). Using a 10% MeOH/DCM mixture as eluent for the column as well as for the TLC, the third fraction was collected (Rf = 0.3) to obtain the pure product as an dark orange solid (37%, 92 mg). ESI-MS m/z (calc): 678.4 (678.3 $[M+H]^+$). ^{1}H NMR (300 MHz, DMSO-d^6) δ 10.48 (d, J = 1.4 Hz, 2H; NH), 9.36 (dd, J = 8.9, 4.6 Hz, 2H; H-4), 9.07-8.98 (m, 2H; H-3), 8.95 (s, 1H; O=C–NH), 8.82 (s, 1H; H-15), 8.36 (dd, J = 8.1, 4.8 Hz, 4H; H-10, 12, 13), 7.84 (dd, J = 8.9, 4.7 Hz, 2H; H-7), 7.58–7.43 (m, 2H; H-8), 7.09–6.97 (m, 2H; H-9), 1.61 (t, J = 20.6 Hz, 2H; H-γ), 1.43–1.05 (m, 18H; H-δ), 0.97–0.69 (m, 3H; H-ε). Elemental analysis calcd (%) for $C_{41}H_{43}N_9O{\cdot}H_2O$: C 70.77, H 6.52, N 18.12; found: C 71.11, H 6.52, N 18.12.

Preparation of an 0.1 M iron(II) stock solution: KSCN (195 mg, 2.00 mmol) and ascorbic acid (6.1 mg, 0.035 mmol) were placed under argon in a round-bottom flask. $FeSO_4{\cdot}7H_2O$ (152 mg, 1.00 mmol) was added and the mixture was suspended in degassed methanol (6.0 mL). The suspension was stirred for 40 min, filtered, and the filtrate was transferred into a volumetric flask. The volume was adjusted to 10.0 mL with degassed methanol and the volumetric flask was well shaken, which resulted in an 0.1 M $[Fe(NCS)_2]$ solution in methanol. Since the filtration and the solution were not kept under argon, the solution had to be prepared fresh for every synthesis. Aerial oxidation of the iron-containing solution was visible due to a change of color (from colorless to dark violet).

[Fe(1)(NCS)$_2$] (2): Compound **1** (8.0 mg, 12 μmol) was put under argon and degassed MeOH (2.0 mL) and $Fe(NCS)_2$ (0.13 mL of 0.1 M stock solution, 13 μmol) were added successively. After refluxing under argon for 12 h at 80 °C the brown precipitate was collected and was washed extensively with MeOH. Compound **2** was obtained as a brown solid (40%, 5.7 mg). HR-MS m/z (calc): 678.36630 (678.36633, **1**$^+$), 366.6464 (366.6465 $[M\text{-}2NCS]^{2+}$), 846.2788 (846.2786 $[M\text{-}2NCS+CF_3COO]^+$). IR ν (cm^{-1}): 3249, 3074, 2922, 2852, 2077 (NCS^-), 1628, 1594, 1545, 1521, 1469, 1417, 1386, 1356, 1242, 1141, 1008, 837,768, 753, 648, 604, 509. Elemental analysis calcd (%) for $C_{43}H_{43}FeN_{11}OS_2{\cdot}5CH_3OH$: C 57.08, H 6.29, N 15.25; found: C 57.96, H 6.08, N 13.73.

Magnetic susceptibility measurement: Magnetic susceptibility measurements were recorded on a Quantum Design MPMS-XL SQUID magnetometer. Prior to the measurements 3.12 mg of compound **2** was centered in a field of 0.1 T at 300 K, then DC magnetization measurements were performed in a field of 0.1 T, from 5 to 350 K (heating mode) and from 350 to 5 K (cooling mode) with a rate of 0.3–1.1 Kmin^{-1}. The measuring time was 20 h, and corrections for the diamagnetism were calculated using Pascal's constants.[60] The measurement was performed within a temperature range of 5 to 350 K with steps of 5 K in the low temperature range and with steps of 2 K in the 250 and 350 K temperature range. At each temperature, the magnetic susceptibility was measured 4 times, to compensate for any measuring errors.

HOPG sample preparation: a drop (9 μL) of a solution of compound **1** or **2** in distilled and degassed DMF (concentration 8×10^{-8} M) was carefully placed on a freshly cleaved HOPG surface under argon. The HOPG surface had been imaged with atomic resolution for reference. The functionalized substrate was then dried under a gentle stream of argon in a Schlenk flask, for over 16 h in the dark. Then the sample was directly probed by STM under ambient conditions.

STM spectroscopy: a PicoSPM I (Agilent Technologies) equipped with an E-scanner (8048 EV) and a Digital Instruments Multimode Microscope (Veeco) with Nanoscope IIIa controller were used to carried out all measurements under ambient conditions. Mechanical vibration was minimized using active vibration isolation table in a home-made sound box. The highly oriented pyrolytic graphite (HOPG, SPI-3, from SPI Supplies) was freshly cleaved using Scotch tape. The graphite surface was then imaged by STM to confirm the high resolution of the tip, and the flatness of the substrate. Mechanically cut Pt-Ir tips (90/10, from Goodfellow Cambridge Limited) of diameter 0.25 mm were used. Typically, the tunneling current set point was 1 nA. The bias voltage was +500 mV. The scan frequency was varied between 0.5 and 3 Hz depending on the scan size. Obtained STM images were flattened to eliminate unwanted features from scan lines (*e.g.*, noise, bow and tilt), and this image analysis command was carried out by using the program NanoScope Analysis (Version 1.40, Bruker Corporation, 2012).

DFT calculations: molecular structures of **1** and **2** were built with MOLDEN and minimized in vacuum using the B3LYP functional and the LANL2DZ basis set for all atoms as implemented in the GAMESS-UK package.

Acknowledgements

Frederica Galli is kindly acknowledged for expert advice on STM. Prof. Lies Bouwman is wholeheartedly acknowledged for scientific discussion and overall support.

Conflict of Interest

The authors declare no conflict of interest.

Keywords: Iron · Molecular materials · Scanning tunneling microscopy · Self-assembly · Surface chemistry

[1] P. Gütlich, H. A. Goodwin, *Top. Curr. Chem.* **2004**, *233*, 3–35.
[2] K. Senthil Kumar, M. Ruben, *Coord. Chem. Rev.* **2017**, *346*, 176–205.
[3] G. Molnár, S. Rat, L. Salmon, W. Nicolazzi, A. Bousseksou, *Adv. Mater.* **2018**, *30*, 1703862.
[4] K. S. Kumar, M. Ruben, *Angew. Chem. Int. Ed.* **2019**, *59*, 2–22.
[5] M. D. Manrique-Juarez, S. Rat, F. Mathieu, D. Saya, I. Séguy, T. Leïchlé, L. Nicu, L. Salmon, G. Molnár, A. Bousseksou, *Appl. Phys. Lett.* **2016**, *109*, 061903.
[6] M. D. Manrique-Juárez, F. Mathieu, A. Laborde, S. Rat, V. Shalabaeva, P. Demont, O. Thomas, L. Salmon, T. Leichle, L. Nicu, G. Molnár, A. Bousseksou, *Adv. Funct. Mater.* **2018**, *28*, 1801970.
[7] H. J. Shepherd, I. y. A. Gural'skiy, C. M. Quintero, S. Tricard, L. Salmon, G. Molnár, A. Bousseksou, *Nat. Commun.* **2013**, *4*, 2607.
[8] C. Bartual-Murgui, A. Akou, C. Thibault, G. Molnár, C. Vieu, L. Salmon, A. Bousseksou, *J. Mater. Chem. C* **2015**, *3*, 1277–1285.
[9] C.-M. Jureschi, J. Linares, A. Boulmaali, P. R. Dahoo, A. Rotaru, Y. Garcia, *Sensors* **2016**, *16*.
[10] K. Boukheddaden, M. H. Ritti, G. Bouchez, M. Sy, M. M. Dîrtu, M. Parlier, J. Linares, Y. Garcia, *J. Phys. Chem. C* **2018**, *122*, 7597–7604.
[11] A. Holovchenko, J. Dugay, M. Giménez-Marqués, R. Torres-Cavanillas, E. Coronado, H. S. J. van der Zant, *Adv. Mater.* **2016**, *28*, 7228–7233.
[12] A. Galet, A. B. Gaspar, M. C. Muñoz, G. V. Bukin, G. Levchenko, J. A. Real, *Adv. Mater.* **2005**, *17*, 2949–2953.
[13] C. Lefter, V. Davesne, L. Salmon, G. Molnár, P. Demont, A. Rotaru, A. Bousseksou, *Magnetochemistry* **2016**, *2*.
[14] T. Miyamachi, M. Gruber, V. Davesne, M. Bowen, S. Boukari, L. Joly, F. Scheurer, G. Rogez, T. K. Yamada, P. Ohresser, E. Beaurepaire, W. Wulfhekel, *Nat. Commun.* **2012**, *3*, 938.
[15] E. P. van Geest, K. Shakouri, W. Fu, V. Robert, V. Tudor, S. Bonnet, G. F. Schneider, *Adv. Mater.* **2020**, *32*, 1903575.

[16] J. Dugay, M. Giménez-Marqués, T. Kozlova, H. W. Zandbergen, E. Coronado, H. S. J. van der Zant, *Adv. Mater.* **2015**, *27*, 1288–1293.
[17] F. Prins, M. Monrabal-Capilla, E. A. Osorio, E. Coronado, H. S. J. van der Zant, *Adv. Mater.* **2011**, *23*, 1545–1549.
[18] J. Dugay, M. Aarts, M. Giménez-Marqués, T. Kozlova, H. W. Zandbergen, E. Coronado, H. S. J. van der Zant, *Nano Lett.* **2017**, *17*, 186–193.
[19] A. Bousseksou, G. Molnar, L. Salmon, W. Nicolazzi, *Chem. Soc. Rev.* **2011**, *40*, 3313–3335.
[20] S. Usmani, M. Mikolasek, A. Gillet, J. Sanchez Costa, M. Rigoulet, B. Chaudret, A. Bousseksou, B. Lassalle-Kaiser, P. Demont, G. Molnár, L. Salmon, J. Carrey, S. Tricard, *Nanoscale* **2020**, *12*, 8180–8187.
[21] H. Li, H. Peng, *Curr. Opin. Colloid Interface Sci.* **2018**, *35*, 9–16.
[22] H. J. Shepherd, G. Molnár, W. Nicolazzi, L. Salmon, A. Bousseksou, *Eur. J. Inorg. Chem.* **2013**, *2013*, 653–661.
[23] S. Hayami, M. R. Karim, Y. H. Lee, *Eur. J. Inorg. Chem.* **2013**, *2013*, 683–696.
[24] S. Schlamp, P. Thoma, B. Weber, *Eur. J. Inorg. Chem.* **2012**, *2012*, 2759–2768.
[25] I. Galadzhun, R. Kulmaczewski, N. Shahid, O. Cespedes, M. J. Howard, M. A. Halcrow, *Chem. Commun.* **2021**, *57*, 4039–4042.
[26] J. Weihermüller, S. Schlamp, W. Milius, F. Puchtler, J. Breu, P. Ramming, S. Hüttner, S. Agarwal, C. Göbel, M. Hund, G. Papastavrou, B. Weber, *J. Mater. Chem. C* **2019**, *7*, 1151–1163.
[27] S. Schlamp, P. Thoma, B. Weber, *Chem. Eur. J.* **2014**, *20*, 6462–6473.
[28] D. Rosario-Amorin, P. Dechambenoit, A. Bentaleb, M. Rouzières, C. Mathonière, R. Clérac, *J. Am. Chem. Soc.* **2018**, *140*, 98–101.
[29] M. Seredyuk, A. B. Gaspar, V. Ksenofontov, Y. Galyametdinov, J. Kusz, P. Gütlich, *Adv. Funct. Mater.* **2008**, *18*, 2089–2101.
[30] M. Seredyuk, A. B. Gaspar, V. Ksenofontov, S. Reiman, Y. Galyametdinov, W. Haase, E. Rentschler, P. Gütlich, *Chem. Mater.* **2006**, *18*, 2513–2519.
[31] S. Hayami, Y. Komatsu, T. Shimizu, H. Kamihata, Y. H. Lee, *Coord. Chem. Rev.* **2011**, *255*, 1981–1990.
[32] J. A. Real, A. B. Gaspar, M. C. Munoz, *Dalton Trans.* **2005**, *34*, 2062–2079.
[33] D. Gatteschi, R. Sessoli, *Angew. Chem. Int. Ed.* **2003**, *42*, 268–297; *Angew. Chem.* **2003**, *115*, 278–309.
[34] A. Mourran, U. Ziener, M. Moller, E. Breuning, M. Ohkita, J. M. Lehn, *Eur. J. Inorg. Chem.* **2005**, *2005*, 2641–2647.
[35] G. G. Condorelli, A. Motta, I. L. Fragalà, F. Giannazzo, V. Raineri, A. Caneschi, D. Gatteschi, *Angew. Chem. Int. Ed.* **2004**, *43*, 4081–4084; *Angew. Chem.* **2004**, *116*, 4173–4176.
[36] S. Bonnet, M. A. Siegler, J. S. Costa, G. Molnar, A. Bousseksou, A. L. Spek, P. Gamez, J. Reedijk, *Chem. Commun.* **2008**, 5619–5621.
[37] H. Spiering, T. Kohlhaas, N. Romstedt, A. Hauser, C. Bruns-Yilmaz, J. Kusz, P. Gütlich, *Coord. Chem. Rev.* **1999**, *192*, 629–647.
[38] O. Kahn, C. J. Martinez, *Science* **1998**, *279*, 44–48.
[39] J. Frey, T. Kraus, V. Heitz, J.-P. Sauvage, *Chem. Eur. J.* **2007**, *13*, 7584–7594.
[40] T. Ishi-i, R. Hirashima, N. Tsutsumi, S. Amemori, S. Matsuki, Y. Teshima, R. Kuwahara, S. Mataka, *J. Org. Chem.* **2010**, *75*, 6858–6868.
[41] M. Ikeda, H. Nakagawa, T. Suzuki, N. Miyata, *Bioorg. Med. Chem. Lett.* **2012**, *22*, 1949–1952.
[42] A. Greguric, I. D. Greguric, T. W. Hambley, J. R. Aldrich-Wright, J. G. Collins, *Dalton Trans.* **2002**, *31*, 849–855.
[43] S. Bonnet, G. b. Molnár, J. Sanchez Costa, M. A. Siegler, A. L. Spek, A. Bousseksou, W.-T. Fu, P. Gamez, J. Reedijk, *Chem. Mater.* **2009**, *21*, 1123–1136.
[44] J. P. Rabe, S. Buchholz, *Phys. Rev. Lett.* **1991**, *66*, 2096–2099.
[45] J. P. Rabe, S. Buchholz, *Science* **1991**, *253*, 424–427.
[46] T. Nakanishi, H. Takahashi, T. Michinobu, M. Takeuchi, T. Teranishi, K. Ariga, *Colloids Surf. A* **2008**, *321*, 99–105.
[47] A. Stabel, J. P. Rabe, *Synth. Met.* **1994**, *67*, 47–53.
[48] A. Hauser, *Top. Curr. Chem.* **2004**, *234*, 155–198.
[49] H. A. Goodwin, K. H. Sugiyarto, *Chem. Phys. Lett.* **1987**, *139*, 470–474.
[50] C. P. Kohler, R. Jakobi, E. Meissner, L. Wiehl, H. Spiering, P. Gutlich, *J. Phys. Chem. Solids* **1990**, *51*, 239–247.
[51] Z. Arcis-Castíllo, S. Zheng, M. A. Siegler, O. Roubeau, S. Bedoui, S. Bonnet, *Chem. Eur. J.* **2011**, *17*, 14826–14836.
[52] S. Zheng, M. A. Siegler, J. Sánchez Costa, W.-T. Fu, S. Bonnet, *Eur. J. Inorg. Chem.* **2013**, *2013*, 1033–1042.
[53] M. F. Guest, I. J. Bush, H. J. J. Van Dam, P. Sherwood, J. M. H. Thomas, J. H. Van Lenthe, R. W. A. Havenith, J. Kendrick, *Mol. Phys.* **2005**, *103*, 719–747.
[54] E. N. Voloshina, D. Mollenhauer, L. Chiappisi, B. Paulus, *Chem. Phys. Lett.* **2011**, *510*, 220–223.
[55] J. D. Wuest, A. Rochefort, *Chem. Commun.* **2010**, *46*, 2923–2925.
[56] C. F. Macrae, I. J. Bruno, J. A. Chisholm, P. R. Edgington, P. McCabe, E. Pidcock, L. Rodriguez-Monge, R. Taylor, J. van de Streek, P. A. Wood, *J. Appl. Crystallogr.* **2008**, *41*, 466–470.
[57] P. N. Martinho, T. Lemma, B. Gildea, G. Picardi, H. Müller-Bunz, R. J. Forster, T. E. Keyes, G. Redmond, G. G. Morgan, *Angew. Chem. Int. Ed.* **2012**, *51*, 11995–11999; *Angew. Chem.* **2012**, *124*, 12161–12165.
[58] A. M. Ako, M. S. Alam, M. Rahman, J. P. Hill, N. M. Sanchez-Ballester, K. Ariga, G. Buth, C. E. Anson, A. K. Powell, *Chem. Eur. J.* **2012**, *18*, 16419–16425.
[59] H. C. Guo, R. H. Zheng, H. J. Jiang, *Org. Prep. Proced. Int.* **2012**, *44*, 392–396.
[60] G. A. Bain, J. F. Berry, *J. Chem. Educ.* **2008**, *85*, 532–536.

Manuscript received: April 12, 2021
Revised manuscript received: June 8, 2021
Accepted manuscript online: June 11, 2021